Soft Matter

PAPER

View Article Online
View Journal | View Issue

Cite this: *Soft Matter*, 2016, 12, 4932

The effect of charge separation on the phase behavior of dipolar colloidal rods

David M. Rutkowski,[a] Orlin D. Velev,[a] Sabine H. L. Klapp[b] and Carol K. Hall*[a]

Received 5th February 2016,
Accepted 28th April 2016

DOI: 10.1039/c6sm00317f

www.rsc.org/softmatter

Colloids with anisotropic shape and charge distribution can assemble into a variety of structures that could find use as novel materials for optical, photonic, electronic and structural applications. Because experimental characterization of the many possible types of multi-shape and multipolar colloidal particles that could form useful structures is difficult, the search for novel colloidal materials can be enhanced by simulations of colloidal particle assembly. We have simulated a system of dipolar colloidal rods at fixed aspect ratio using discontinuous molecular dynamics (DMD) to investigate how the charge separation of an embedded dipole affects the types of assemblies that occur. Each dipolar rod is modeled as several overlapping spheres fixed in an elongated shape to represent excluded volume and two smaller, embedded spheres to represent the charges that make up the extended dipole. Large charge separations predominately form structures where the rods link head-to-tail while small charge separations predominately form structures where the rods stack side-by-side. Rods with small charge separations tend to form dense aggregates while rods with large charge separations tend to form coarse gel-like structures. Structural phase boundaries between fluid, string-fluid, and "gel" (networked) phases are mapped out and characterized as to whether they have global head-to-tail or global side-by-side order. A structural coarsening transition is observed for particles with large charge separations in which the head–tail networks thicken as temperature is lowered due to an increased tendency to form side-by-side structures. Triangularly connected networks form at small charge separations; these may be useful for encapsulating smaller particles.

Introduction

Colloidal particles can assemble into a rich variety of structures that hold promise for application in biotechnology,[1–3] photonics,[4–7] and electronics or computation.[8–10] When the shape, surface coating or internal charge distribution of the particles are anisotropic, the diversity of possible structures becomes even richer, offering enhanced opportunities for tuning the local order, leading to interesting and novel colloidal architectures including chains, crystals, gels and ribbons.[11] Particles with anisotropic shape including suspensions of rod-shaped particles[12] can form both nematic and smectic phases, a feature useful in display devices.[13] Similarly, patchy particles including Janus particles can self-assemble into a multitude of different phases including giant micelles and bilayers.[14] These anisotropies can be manipulated through imposition of external fields leading to even better control over the structures formed.[15–18]

Not surprisingly, colloidal particles with anisotropic charge distributions exhibit complex phase behavior. Distributions of electric or magnetic charges in a colloidal particle can be treated as one or more embedded dipoles. The simplest type of colloidal particle with charge distribution is the dipolar sphere which has a single point-dipole located in its center. The anisotropic distribution of charge on dipolar spheres leads to a propensity to form chains, especially in response to external electric fields and, as a consequence, holds promise for creating photonic crystals with novel symmetries, electrical materials, and water-based electrorheological fluids.[11,19,20] Manipulating these chains with external electric or magnetic fields may allow for the formation of materials with switchable properties such as switching from radiation absorber to reflectors.[11] Here we consider dipolar rods – colloidal particles with anisotropies in both shape and charge distribution – to obtain a basic understanding of how these two factors combine to yield interesting phase diagrams.

Dipolar colloidal rods display more complex phase behavior than particles with only one form of asymmetry, such as dipolar spherical particles or rod-shaped particles. For example, electrically dipolar rods have been created experimentally by Zhang *et al.* using PRINT which they found aligned in a head-to-tail fashion along an external electric field.[21] Kozek *et al.* have synthesized nano-meter sized dipolar rods by coating a gold rod in silica and then attaching a magnetic overcoat to the silica layer.

[a] *Department of Chemical & Biomolecular Engineering, North Carolina State University, Raleigh, NC 27695, USA. E-mail: hall@ncsu.edu*
[b] *Institute of Theoretical Physics, Technical University of Berlin, Secr. EW 7-1 Hardenberstr. 36, D-10623 Berlin, Germany*

These particles have been found to align with an external electric field.[22] Magnetic dipolar rods can be created experimentally by methods such as covering silica rods with a thin layer of nickel so that the rods become magnetically responsive.[23] These rods have been found to form cyclical structures that are responsive to an external field. Gold nanorods synthesized by Fava *et al.* with cetyl trimethyl ammonium bromide (CTAB) on the sides and polystyrene molecules (PS) on the ends assemble into chains, side–side oriented chains, raft structures, and even spheres, depending on solvent quality.[24] Nanorods which instead have poly(*N*-isopropylacrylamide) (PNIPAm) on the ends, have been found to photothermally self-assemble into chains.[25] Many of the techniques used for fabricating multipolar particles suffer from either low yields or high polydispersity, limiting the practicality of experimentally investigating the bulk phase properties of these particles.[19] As a consequence, most experimental and many simulation investigations, including this work, focus on the behavior of dipolar colloidal rods at surfaces.

A number of simulation techniques have been used to investigate the phase behavior of colloidal particles that are either rod-like, dipolar or both. Bolhuis and Frenkel found using a combination of Monte Carlo techniques and Gibbs–Duhem integration that the phase diagram for hard rods is highly dependent on their aspect ratio, displaying a nematic phase and smectic phase at moderate aspect ratios and densities.[12] McGrother and Jackson used both canonical and Gibbs ensemble Monte Carlo (GEMC) to simulate a system of dipolar spherocylinders with a point dipole embedded in the center and found evidence for vapor–liquid coexistence as the aspect ratio increased.[26] Alvarez and Klapp applied Monte Carlo simulations to systems of dipolar rods with permanent magnetic dipole moments modeled as fused magnetic dipolar spheres.[27] Additionally, they investigated rod-like particles with a longitudinal point dipole and found clusters of parallel rods as we do in our simulations at low charge distances.[28] Miller *et al.* used molecular dynamics to investigate systems of dipolar dumbbells, representing the dipole–dipole interaction by a combination of a soft-sphere interaction and Coulombic interaction, and found that these particles aligned into head-to-tail chains.[29] Schmidle *et al.* performed simulations of two dimensional systems of dipolar spheres in the presence of electric fields and found close agreement between the structures formed in simulation and the experimentally observed structure formed by similar particles.[30,31] Goyal *et al.* showed using discontinuous molecular dynamics (DMD) simulations that three-dimensional systems of spherical dipolar colloidal particles[32] form a number of phases including low volume fraction gels and high volume fraction hexagonally-close-packed, body centered tetragonal and face-centered cubic phases. Additionally, they found that mixtures of these particles formed bicontinuous gels.[33] Like Goyal *et al.* we have used a short-ranged potential designed to mimic electrostatic charges interacting in a high salt solution.

The long term goal of our investigation into the phase behavior of colloidal particles *via* molecular-level computer simulations is to screen the many types of structures formed by anisotropic particles so as to identify the ones that would be of interest for advanced applications. Molecular simulation has an advantage over experiment in this regard because precisely defined, monodisperse "molecules" of virtually any type can be generated. In contrast, many of the techniques for fabricating particles, including microcontact printing, Pickering emulsion techniques, and oil water emulsion techniques, cannot produce large quantities of monodisperse particles.[19] This makes it hard to identify the specific molecular features which are responsible for the behaviors of the particles. An attractive alternative, therefore, is to first identify interesting structures through computer simulation and then to explore these structures more precisely through experimentation.

The objective of the current research is to systematically investigate how the internal charge separation of dipolar colloidal rods affects the types of assemblies that occur over a range of temperatures and densities with the internal charge separation of the extended dipole being the control parameter. While others have investigated dipolar colloidal rods through simulation, the focus has usually been on how the aspect ratio of the rod affects the phase behavior[27,34] instead of how the internal charge separation affects the phase behavior, as we focus on in this work. A key consideration in the types of assemblies that form is the alignment of the particles at different conditions. A pair of rods can in general align in two orientations: either head-to-tail or side-by-side.[26,27,34] In our model a shift between these two orientations occurs when the charge separation is varied. The exact charge separation value that defines the boundary between these two orientations depends on both the aspect ratio of the rod and the expression for the potential energy of interaction between the electric charges, herein represented by a screened Coulomb potential, *i.e.* a Yukawa potential. A Yukawa potential was chosen because it allows for a faster evolution of the system than would a Coulomb potential with long range interactions. The simulations approach is used to map out the conditions under which a system of 2-d dipolar rods will predominantly align side-by-side or head-to-tail. While it can easily be determined if an isolated pair of particles will form head–tail or side–side pairs, the details of where these transitions occur in many particle systems and whether there are any other structural transitions is more challenging to discern without performing simulations.

Simulations of systems of dipolar particles can be classified according to how the dipole moment is represented: by a point dipole or by an extended dipole. Those simulations implementing a point dipole representation use the standard expression for the dipole–dipole interaction potential and are more suitable when the separation between the charges of the dipole is small.[26] The expression breaks down when the interparticle separation is on the same order of magnitude as the separation between the charges that make up the dipole. This can be dealt with by either adding higher order terms to the expansion, *e.g.* quadrupolar, octapolar, *etc.*, or by explicitly modeling the individual charges with an extended dipole.[35] Simulations with extended dipoles typically use a form of the Coulomb potential between the individual positive and negative charges on different molecules[29,36] and are more appropriate when the two charges are separated

by a distance on the same order or greater than the distance separating the centers of the dipoles. Dipolar spheres with embedded, extended dipoles have been used in simulation to learn how the charge separation affects the phase behavior.[35,37] Simulations of dipolar rods with extended dipoles have also been performed but, as mentioned earlier, these have focused on how the aspect ratio of the rods, not the charge separation alone, affects the phase behavior.[36] Because we are interested in how changing the charge separation within a dipolar rod affects phase behavior, we have chosen to explicitly model the charges on the dipole rather than use a point dipole representation.

The method we have chosen to use for our simulations of dipolar rods is discontinuous molecular dynamics simulations (DMD). Unlike typical molecular dynamics (MD) simulations in which the interaction between two particles is represented by a continuous function of the inter-particle distance, DMD uses potentials that are a discontinuous function of the inter-particle distance. The advantage of using a discontinuous potential is that when two particles are between discontinuities nothing needs to be calculated and the particles move ballistically. The particle velocities change only when the two particles reach a discontinuity. As a consequence, DMD moves through time by advancing between "collision" events rather than using a fixed time step as in MD. For this reason, DMD is an event-driven algorithm; it uses an event scheduling queue to determine the soonest to occur collision in the system and then updates the entire system to that time. The DMD algorithm is a much faster procedure than calculating the potential between each particle at the discrete uniformly-spaced time steps associated with MD. This speedup allows the simulation of longer timescales than would typically be possible and is applicable to our system since rods take longer time to achieve their equilibrium state than spheres due to their extra rotational modes.

In this paper we present results from DMD simulations of dipolar rods modeled as spherocylinders with a length to width ratio of 4 : 1 for four values of the charge separation to width ratio (2.5, 3.0, 3.5, and 3.7). Our simulations were performed in 2-d, where 2-d means a two dimensional simulation box, to better correspond with experiments in which colloidal particles are placed on a glass slide or have sedimented onto a surface.[19,38] Since we are interested only in the general phase behavior of dipolar colloidal rods we have not modeled a specific system, but have developed a system guided by experimentally feasible parameters. We investigate the conditions at which the fluid phase, the string-fluid phase, the "gel" phase, the head-to-tail ordered phase, and the side-by-side ordered phase occur. The definitions of these phases are described in the Model and methods section.

Our results include the following highlights. Phase diagrams in the area fraction *vs.* temperature plane have been calculated for all four charge separations investigated (2.5, 3.0, 3.5 and 3.7) which delineate boundaries between the three main phases investigated (fluid, string-fluid and "gel") along with other transitions indicating the development of head–tail and side–side ordering. We also discovered a structural coarsening transition for systems of particles with charge separations 3.5 and 3.7; where structural coarsening refers to the thickening of network structures as head–tail "gels" formed at intermediate temperatures additionally form side–side structures at low temperatures. Rods with a charge separation of 3.0 form a mixed side–side and head–tail "gel" at low temperatures, which does not seem to be the equilibrium structure, suggesting the rods are dynamically arrested in a metastable state. Rods that form head–tail aggregates percolate at higher temperatures than those that form side–side structures, with the shortest charge separation, 2.5, percolating only at intermediate area fractions.

Model and method

We represented our 4 : 1 aspect ratio dipolar rod by a group of seven overlapping spheres, which are each separated from their nearest neighbor by a distance of 0.5σ resulting in an aspect ratio of 4 : 1; the spheres are bonded together to approximate the rod shape as shown in Fig. 1. We chose to use an aspect ratio of 4 : 1 since this is closest to nanorods created by Wu and Tracy.[39] We chose to use a distance of 0.5σ arbitrarily, but found it resulted in a small difference between the area of a true spherocylinder and our model as discussed in our conclusions section. Seven spheres are used based on the aspect ratio and distance between nearest spheres in the rod. Since DMD is an event-driven simulation technique, it is significantly easier to find collision times between particles if the particles are spheres rather than another shape. The positive and negative charges are represented by two smaller spheres embedded at selected locations near the ends of the dipolar rod; hence this is an extended dipole representation. The larger spheres have a diameter of σ while the smaller spheres representing the charges have a diameter of 0.3σ. The smaller spheres were chosen to have a diameter of 0.3σ to correspond with work performed previously by Goyal *et al.*, but were otherwise chosen arbitrarily.[32] These larger spheres do not interact with each other on the same chain, and are bonded to nearest neighbors and next nearest neighbors using the method of Bellemans. The length of the bonds between neighboring spheres varies between $(1 - \delta)\sigma$ and $(1 + \delta)\sigma$ where σ is the length of the bond between the centers of the spheres and δ is the so-called Bellemans' constant which is used to define how tightly the spheres are bound to each other.[40]

In our simulations we set δ equal to 7.654×10^{-3} in reduced units of length, which serves to keep the rod relatively straight,

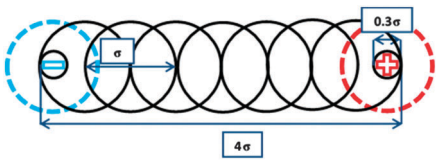

Fig. 1 Model of 4 : 1 dipolar rod used in our DMD simulations incorporating seven spheres bonded together to represent the excluded volume of the rod and two smaller spheres shown in red and blue at the ends to represent the charges of the extended dipole. The outermost square wells for the charged spheres are shown as dashed circles.

and keeps the angle between the center sphere and the two end spheres of the rod greater than or equal to 170 degrees. The Bellemans' constant for the smaller spheres is the same as that for the large spheres so that all the distances are consistent (*i.e.* all bonds can be at either their shortest or longest distance without any bond overlapping). The small spheres are bonded to the large sphere at the end of the rod that they are closest to. They are also bonded to each other so that they maintain their position within the rod. The small spheres are used only to localize the centers of the charge and do not interact with the uncharged spheres except through bonds within the rod.

The small spheres in different rods interact with each other *via* a square well (*i.e.* attractive) potential if the charges that the spheres represent are of opposite sign while they interact with a square shoulder (*i.e.* repulsive) potential if the charges are of the same sign. The square shoulder has the same boundaries and magnitude as the square well, but has positive energies instead of negative ones. The pair potential between charges on the ends of different rods was modeled as a three-step square-well or square-shoulder potential designed to approximate a Yukawa potential. The Yukawa potential, also known as the screened Coulomb potential, is defined as

$$U(r^*) = -\varepsilon/r^* \exp(-\kappa^*(r^* - 1)) \quad (1)$$

where $U(r^*)$ is the potential energy between a pair of charges with opposite sign, ε is a constant with units of energy related to the strength of the interaction, κ^* is the reduced inverse Debye screening length and r^* is the dimensionless distance, defined as $r^* = r/\sigma$, between two charges.[41] The parameters for the Yukawa potential used in our simulation were chosen to be characteristic of rods with a diameter of 20 nm, the typical size of the gold nano-rods synthesized by Kozek *et al.* and Maity *et al.*,[22,42] and suspended in a solution of 10^{-5} M NaCl. From these values, we calculated the Debye length, $1/\kappa$, to be 96.1 nm using the formula for 1 : 1 electrolytes, $1/\kappa = 0.304/[\mathrm{NaCl}]^{0.5}$, where [NaCl] is the concentration of NaCl in solution.[43] The reduced inverse Debye length, $\kappa^* = \sigma\kappa$, is thus 0.208. The reduced temperature for our simulations is $T^* = \tilde{T}k_BT/\varepsilon$ where k_B is the Boltzmann constant, ε is the constant in the Yukawa potential, and $\tilde{T}$ is equal to 0.864. $\tilde{T}$ was calculated by setting our Yukawa potential equal to a simplified Coulomb potential, $U_C(r^*) = -1/r^*$, at the distance of closest approach for two charged spheres in our simulations, $r^* = 0.3$. The reduced area fraction in our simulations is defined as $\rho^* = \rho\sigma^2$.

For the continuous Yukawa potential just defined, we plot the boundary between head–tail dominated and side–side dominated regions in the reduced charge separation *vs.* rod length parameter space in Fig. 2, creating a ground-state phase diagram for a pair of dipolar rods. This boundary is calculated by equating the total potential energy of a pair of rods in the head–tail configuration and a pair in the side–side configuration to give the charge separation at which the two configurations are equal in energy for a given rod length. This plot has the correct limiting behavior in that it predicts that dipolar spheres, which have a rod length of 1.0, should always form head–tail structures, regardless of the charge separation. For our system of dipolar rods

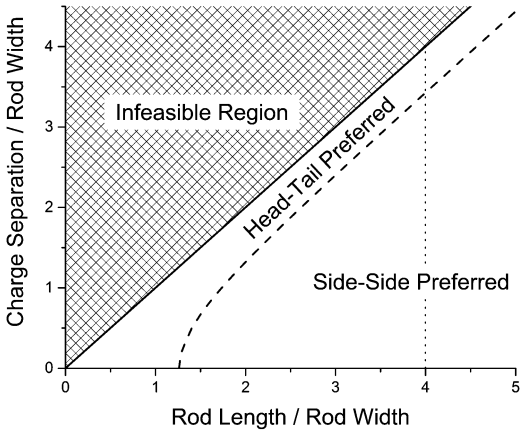

Fig. 2 Plot of charge separation *versus* rod length both reduced by the rod width, which shows the regions where a head–tail pair of dipolar rods is preferred and where a side–side pair of dipolar rods is preferred. The dashed conformation delineation line shifts slightly depending on the potential used to model the interactions between the charged groups in the dipolar rod. The hashed region is infeasible because it has charge separations that are longer than the rod itself. The dotted line indicates the aspect ratio at which the simulations in this paper were performed.

which has an aspect ratio of 4 : 1, the internal charge separation at which the head–tail and side–side configurations have the same interaction energy is 3.43 in reduced units of length.

The full definition of the three step discontinuous potential well used to model the interaction between centers of oppositely-signed charges on each rod is given below. The potential used between charges of the same sign has the same boundaries and energy magnitudes, but opposite signs for the epsilon values defined below, *i.e.* it is a square shoulder.

$$U_{SW}(r) = \begin{cases} \infty & \text{if} \quad r < \sigma_1 \\ -\varepsilon_1 & \text{if} \quad \sigma_1 < r < \sigma_2 \\ -\varepsilon_2 & \text{if} \quad \sigma_2 < r < \sigma_3 \\ -\varepsilon_3 & \text{if} \quad \sigma_3 < r < \sigma_4 \\ 0 & \text{if} \quad r > \sigma_4 \end{cases} \quad (2)$$

The values of the interaction energy parameters are $\varepsilon_1 = 3.129$, $\varepsilon_2 = 1.717$, and $\varepsilon_3 = 0.719$ while the values for the well boundaries are $\sigma_1 = 0.3\sigma$, $\sigma_2 = 0.433\sigma$, $\sigma_3 = 0.595\sigma$, and $\sigma_4 = 1.1\sigma$. A comparison between this discontinuous potential and the Yukawa potential on which it is based is shown below in Fig. 3. In the Appendix we describe the procedure that we used to determine the ε and σ values listed above and the discontinuous potential between oppositely charged small spheres shown in Fig. 3. Here we just point out that the discontinuous charge–charge potential used to mimic the Yukawa potential was chosen not by matching the charge–charge potential directly but by matching the total potential between a pair of dipolar rods, the "rod–rod potential", over a variety of configurations.

We performed simulations at four values of the charge separation, two that should predominately form side–side aggregates, charge separations 2.5 and 3.0, and two that should predominately

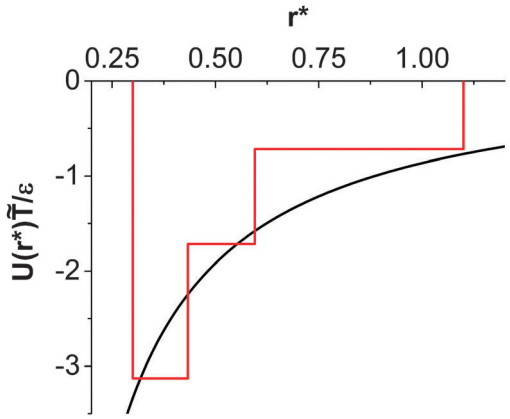

Fig. 3 Plot comparing the continuous Yukawa potential energy and our discontinuous potential energy between charges of opposite sign *versus* the distance between the centers of the two charges. Charges with the same sign interact through a square shoulder that has the same energy boundaries and magnitudes, but has positive values of energy instead of negative.

form head–tail aggregates, charge separations 3.5 and 3.7. The only difference between these simulations was the distance between the charges in the embedded, extended dipole.

For all charge separations we followed the same simulation procedure. Our systems consisted of 500 dipolar rods with aspect ratio 4 : 1 in a square 2-d simulation box with periodic boundary conditions. As with regular MD, DMD is naturally performed in the *NVE* ensemble since energy is conserved between collisions. In order to implement constant temperature, we used the Andersen thermostat, in which a randomly-chosen particle collides with a "ghost" particle so that the system attains a Boltzmann distribution around the desired temperature.[44] We started at a high reduced temperature, $T^* = 5.0$, in order to get a random configuration and then slowly lowered the temperature in a simulated annealing procedure. Simulated annealing allows us to examine structures that are close to equilibrium across a wide range of temperatures. The temperature was lowered in discrete steps; first in steps of 1.0 in reduced units, then steps of 0.1 from 2.0 to 0.30 and finally in steps of 0.01 from 0.30 to 0.01 allowing the system to equilibrate for 100 million collisions at each temperature step. We decrease the temperature in slower increments at lower temperatures because equilibrium takes longer to reach at lower temperatures. We stopped the cooling procedure once the temperature reached a value of 0.01. At this temperature a "gel" or aggregate structure had formed for all rods simulated.

In order to determine what phase the system is in, we need to first define the clustering criterion for our particles. In our simulations we define two rods to be in the same cluster if oppositely charged spheres on this pair are within each other's outermost well, which is 1.1σ. If the charges are of the same sign they are not counted as a pair, since their interaction is repulsive instead of attractive as is required for a cluster to be established. If a rod is determined to be in a cluster with a second rod which is in turn in a cluster with a third rod all three rods will be considered to be in the same cluster. A cluster containing all of the particles in the system is therefore possible.

The percolation probability, Π, gives the probability of finding a spanning or percolating cluster in a given system and is defined as the number of configurations which have a cluster that is percolated, C_{per}, over the total number of configurations investigated, C.

$$\Pi = \langle C_{per}/C \rangle \quad (3)$$

A cluster is percolated if it connects to itself and spans the box, forming a cluster of infinite length when periodic images of the box are included. For a given configuration, the percolation state is 1 if the system is percolated and 0 if the system is not percolated.[45] The percolation probability at a given temperature step in our simulations is the average of this percolation state over 20 configurations at that temperature. The boundary between the "gel" phase, which is associated with a system that is percolated, and the string-fluid phase, which is associated with a system that is not percolated, is determined by locating the inflection point in the percolation probability *vs.* temperature curve. We determined the transition temperature between percolated and non-percolated states by plotting the percolation probability *versus* temperature and then fitting a tanh function to this curve in order to find the inflection point as shown in Fig. 4(a). This inflection point gives the percolation temperature, which is the transition temperature between the string-fluid and "gel" phases.[45]

The extent of polymerization, Φ, gives a measure of when the particles start to associate, and is defined as the ensemble average of the number of rods in the system that are in a cluster, N_a, divided by the number of rods in the system, N,

$$\Phi = \langle N_a/N \rangle \quad (4)$$

The extent of polymerization varies between 0 and 1 since there cannot be more rods in a cluster than the number of rods in the system. The inflection point in a plot of the extent of polymerization *versus* temperature defines the boundary between fluid and string-fluid phases for a given area fraction as shown in Fig. 4(b). In order to find the inflection point, we fit the extent of polymerization *versus* temperature to a logistic5 curve which has the form $\Phi = C_1 + (C_2 - C_1)/(1 + (C_3/T)^{C_4})^{C_5}$ which involves

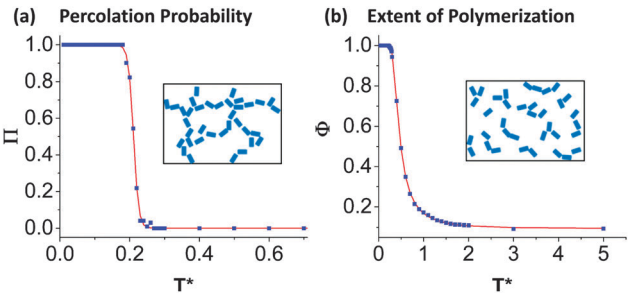

Fig. 4 Order parameters calculated in our simulations along with sample data (blue points) and curves fit to the data (red lines). (a) Percolation probability and an example of a percolated system. (b) Extent of polymerization and an example of a string-fluid.

5 fitting constants (C_1, C_2, C_3, C_4, C_5). We are not suggesting that this function underlies the relationship between the temperature and the extent of polymerization for our system, and have only used this function to get a smooth curve with which to find the inflection point.

Two order parameters were developed to determine whether the system is arranged in a head-to-tail or a side-to-side arrangement. A rod is defined to have a head–tail partner if oppositely charged spheres on nearby rods are less than 1.1σ from each other provided that the remaining two charged spheres are further than 1.1σ from each other. (see Fig. 5(a)) A single rod can have multiple head–tail partners, but our head–tail order parameter only measures whether or not a rod has at least one head–tail partner. The head–tail order parameter, H, is defined as the average number of rods with at least one head–tail partner, N_{H-T}, divided by the number of rods in the system.

$$H = \langle N_{H-T}/N \rangle \quad (5)$$

Like the extent of polymerization, the head–tail order parameter must be between 0 and 1. In order to determine the boundary between non-head–tail ordered and head–tail ordered we fit this order parameter *versus* temperature to a logistic5 curve as shown in Fig. 5(a). The inflection point in this curve was taken to be this boundary.

A rod is defined to have a side–side partner if a pair of oppositely charged spheres on the two rods are less than a distance of 1.1σ from each other and the other two charged spheres are also less than a distance of 1.1σ. (see Fig. 5(b)) As with the head–tail order parameter, a single rod can have multiple side–side partners, but our side–side order parameter only measures whether or not a rod has at least one side–side partner. The side–side order parameter, S, is defined as the average of the number of rods that have at least one side–side partner, N_{S-S}, divided by the number of rods in the system.

$$S = \langle N_{S-S}/N \rangle \quad (6)$$

In order to determine the boundary between non-side–side ordered and side–side ordered we fit this order parameter *versus* temperature to a logistic5 curve. Again the inflection point in this curve *versus* temperature is taken to be the boundary between non-side–side ordered and side–side ordered as shown in Fig. 5(b). Two rods cannot be both a head–tail pair and a side–side pair; the order parameters are defined in a way that they are exclusive of each other.

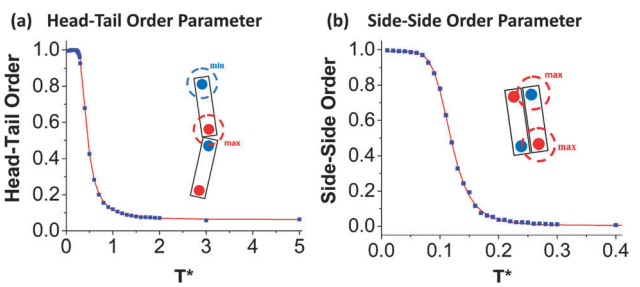

Fig. 5 (a) Head–tail order parameter and an image of a pair of rods that are head–tail ordered. (b) Side–side order parameter and an image of a pair of rods that are side–side ordered.

Results

We present the simulation results for four systems: two that should predominately form head–tail structures (internal charge separations of 3.7 and 3.5) and two that should predominately form side–side structures (internal charge separations of 3.0 and 2.5).

We first present the results for dipolar rods with an internal charge separation of 3.7. The phase diagram for this system plotted in the volume area fraction *versus* temperature plane is shown in Fig. 6. As the system is cooled from a reduced temperature of 5.0, it first transitions from a fluid phase to a string-fluid phase. While each pair making up the clusters in this string-fluid has to be at least head–tail (H–T) ordered or side–side (S–S) ordered, the system as a whole is not considered S–S ordered or H–T ordered until the S–S order parameter or the H–T order parameter displays an inflection point. Thus the string-fluid at intermediate area fractions is neither H–T nor S–S ordered. This globally disordered string-fluid further transitions to a string-fluid with global H–T order, and so is called an H–T string fluid. Upon further cooling the system transitions to an H–T "gel", and then further transitions to a "gel" with both H–T and S–S order. This last transition reflects a coarsening of the overall "gel" structure where the single strands of the

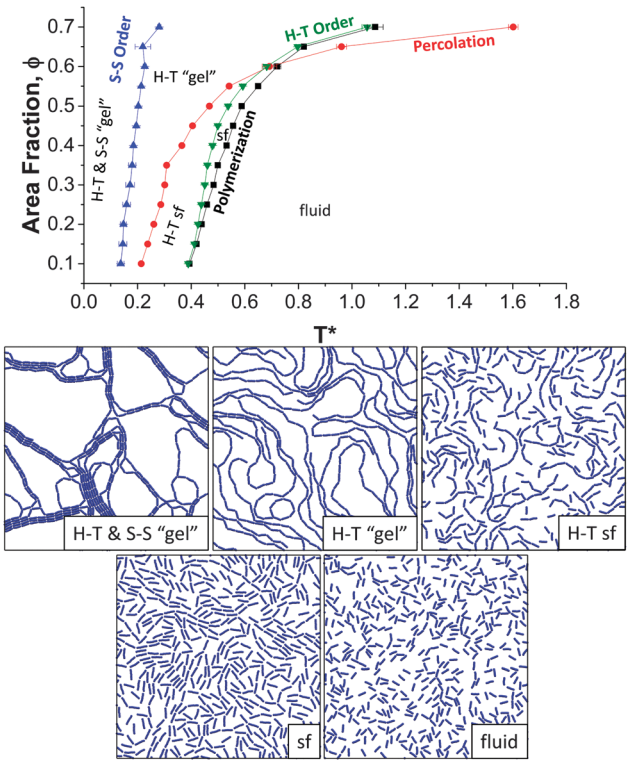

Fig. 6 Phase diagram for 4 : 1 dipolar rods with charge separation of 3.7 plotted in the area fraction *vs.* temperature plane. Fluid, string-fluid, H–T string-fluid, H–T "gel" and H–T & S–S ordered "gel" phases are present in this diagram.

H–T "gel" aggregate together to form S–S aggregates, resulting in a more compact structure. Images of both the head–tail ordered "gel" and the coarser "gel" (H–T and S–S) are shown in Fig. 6 as well along with images of the string-fluid and fluid phases. At high area fractions the percolation line crosses the polymerization line resulting in the system being percolated at a higher temperature than that at which all the rods in the system have partners. This suggests that the system has a percolated group of rods but that not all rods in the system have a partner. A difficulty with this high area fraction region, however, is that the polymerization probability always has a large value even at high temperatures because the particles are forced to be near each other due to area constraints. At higher area fractions, the polymerization probability indicates a transition from a state in which the majority of rods have a partner to a state in which all of the rods have a partner. This is in contrast to lower area fractions where the polymerization probability indicates the transition from a state in which no rods have a partner to a state in which most rods do have a partner. Thus as we increase area fraction our distance based clustering parameters may be misrepresenting where boundaries should occur.

Plots of the S–S order parameter *versus* temperature for charge separation 3.7 rods display a sudden decrease as the temperature is lowered just before the "gel" transition is reached at all area fractions. Before this dip, the S–S order parameter behaves as expected, increasing slightly as the temperature is decreased up to a reduced temperature of around 1. As the temperature is lowered further, the S–S order parameter first decreases and later increases as the "gel" structure coarsens. This dip in the S–S order parameter occurs roughly at the temperature where the H–T order parameter approaches 1. This suggests that the formation of the largest H–T ordered structures depletes some of the S–S partners that existed at higher temperatures. This is the only charge separation and order parameter which displays this behavior.

We next present the results for dipolar rods with an internal charge separation of 3.5. The phase diagram for this system is shown in Fig. 7 It is very similar to that for charge separation of 3.7 with two main exceptions. The first exception is that the globally disordered string-fluid region for charge separation 3.5 exists over a wider range of temperatures than for charge separation 3.7. The second exception is that the H–T order transition is shifted towards lower temperatures especially at higher area fractions. Consequently, this system transitions from a globally disordered gel phase into a H–T "gel" phase at area fractions above 0.35. Like the previous system, this system also displays a "gel" coarsening at the lowest temperatures where the system is a "gel" with both H–T and S–S order. At these low temperatures the S–S order parameter for this system is noticeably higher than for the previous system at the same temperature. This is consistent with the idea that as the charges move closer together the rods are more likely to form S–S pairs even though the dominant pair structure formed should still be H–T for this system. The higher S–S order parameter also results in thicker structures than in the charge separation 3.7 case, since there are more S–S pairs.

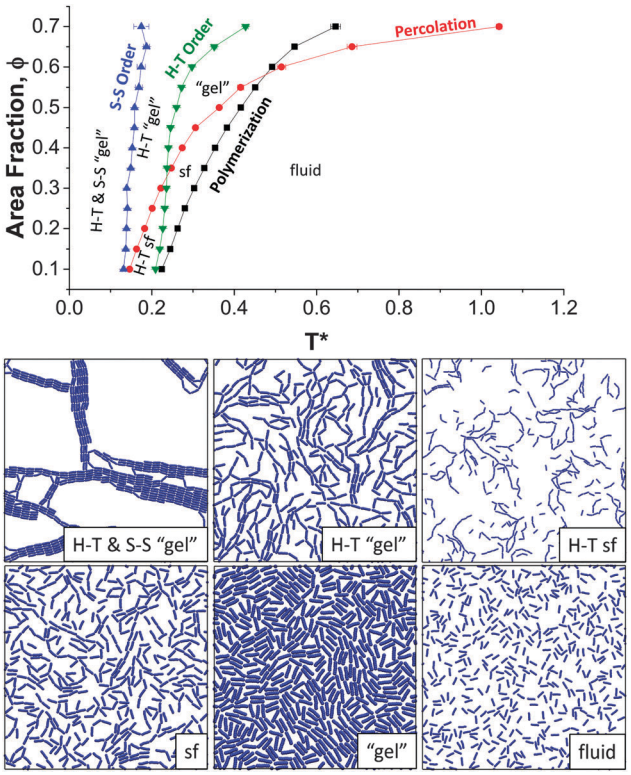

Fig. 7 Phase diagram for dipolar rods with charge separation 3.5 plotted in the area fraction *vs.* temperature plane. Fluid, string-fluid, H–T string-fluid, H–T "gel", "gel", and H–T and S–S "gel" are present.

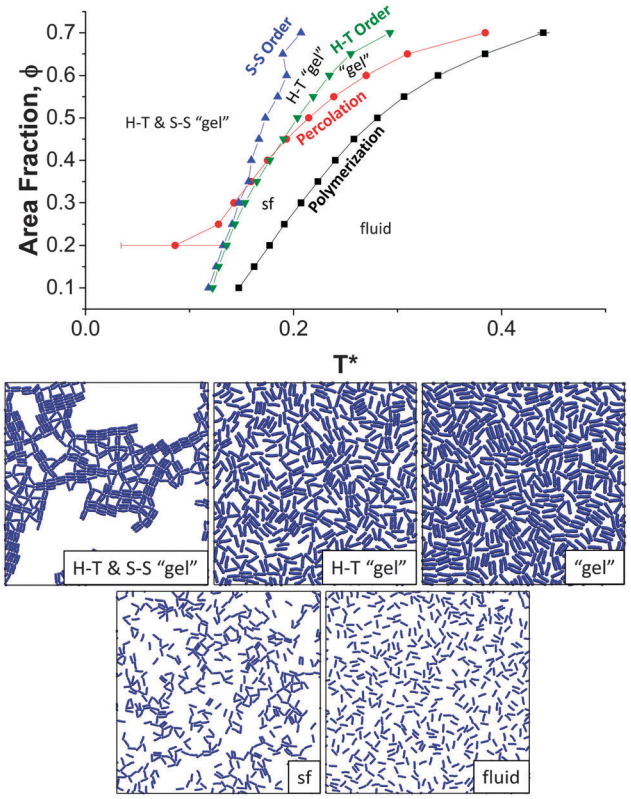

Fig. 8 Phase diagram of dipolar rods with 3.0 charge separation plotted in the area fraction *vs.* temperature plane. Fluid, string-fluid, H–T "gel" and H–T and S–S "gel" are present.

The third system investigated consists of dipolar rods with an internal charge separation of 3.0. This is the first of two systems considered that predominately form S–S structures. The phase diagram for this system is shown in Fig. 8. As the temperature is lowered this system shows a transition from a fluid into a globally disordered string-fluid which, upon further cooling, transitions to a S–S string-fluid at high area fractions or a string-fluid which has both S–S and H–T order at low area fractions. Both of these string-fluids transition directly to a "gel" which has both H–T and S–S order as the temperature is lowered further. The occurrence of this H–T and S–S "gel" phase does not seem to indicate a coarsening as it did in the charge separation 3.5 and 3.7 cases since the "gel" phase that forms has a very open structure with groupings of three rods forming triangular aggregates as can be seen in Fig. 8. While triangular aggregates are unusual for systems of dipolar spheres they have been seen in prior simulations of dipolar rods.[36]

The fourth and final system investigated consists of dipolar rods with an internal charge separation of 2.5. Since the charges on the rods with an internal charge separation of 2.5 are far from the ends of the rods, the rods do not experience any attraction if they are in H–T alignment using our discontinuous potential. This obviously favors the formation of S–S structures. Consequently, this system transitions from a fluid to an S–S string-fluid at all area fractions as can be seen in the phase diagram for this system in Fig. 9. For this system the polymerization probability curve nearly coincides with the S–S order curve, which further indicates the particles are only ordering in an S–S fashion. Upon further cooling and at intermediate area fractions this S–S string-fluid transitions to a coarse S–S "gel". At low area fractions (below 0.25) and at very high area fractions (above 0.60) the system does not have a stable percolation transition. Examples of non-percolated structures at very low and very high area fractions are shown in Fig. 9. The absence of a percolation transition at low area fraction is likely a consequence of the S–S ordering of the system. S–S aggregates have a more difficult time spanning the box than H–T aggregates since the S–S aggregates have smaller aspect ratios than the H–T aggregates We believe that the disappearance of the percolation transition at high area fractions occurs because the system is jammed. The S–S clusters form individual domains instead of long structures which percolate. Although percolated structures may be the true equilibrium structure, our system does not reach this state and becomes stuck in a metastable, non-percolated state. Interestingly, a similar structure has been seen experimentally with rods that have surfactant molecules attached to their sides[46] and in simulations of 2-d spherocylinders.[47]

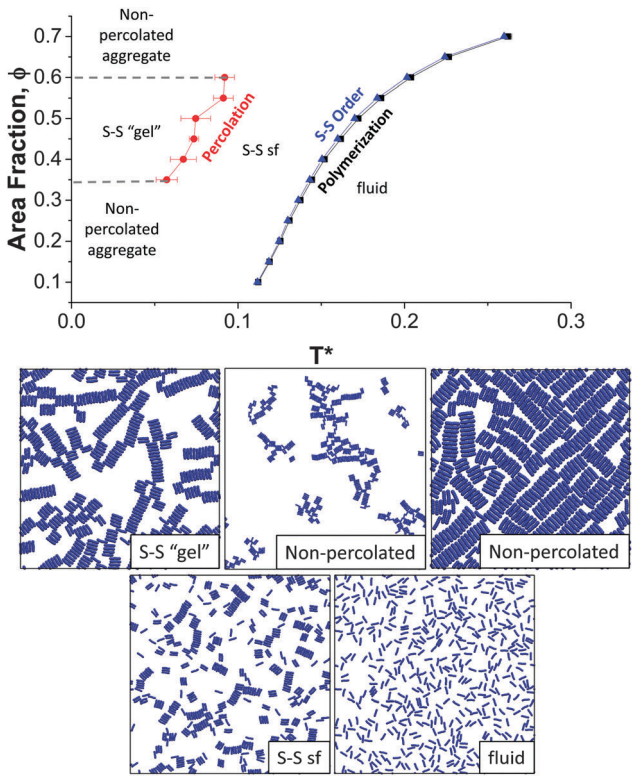

Fig. 9 Phase diagram of dipolar rods with charge separation 2.5 plotted in the area fraction *vs.* temperature plane. Fluid, S–S string-fluid, and S–S "gel" are present. There is no H–T transition for this system; the rods always line up in S–S fashion.

Discussion and conclusions

We have calculated phase diagrams for monodisperse systems of 4 : 1 dipolar colloidal rods with internal charge separations of 3.7, 3.5, 3.0, and 2.5 using discontinuous molecular dynamics simulations with a charge–charge potential that is a discontinuous approximation to a Yukawa potential. These phase diagrams displayed fluid, string-fluid and "gel" phases which were further characterized either by H–T or S–S ordering of the rods. We found a gel coarsening transition for systems of dipolar rods with charge separations of 3.5 and 3.7 which was indicated by an increase in the S–S order parameter. Dipolar rods with charge separations of 3.0 were found to form "gels" with mixed S–S and H–T ordered structures. Dipolar rods with charge separations of 2.5 formed coarse "gels" containing only S–S structures over a limited range of area fractions. Consideration of the four cases discussed indicates that as the charge separation is decreased, the temperature at which the percolation transition occurs shifts to lower values. The main reason for this is that the interactions between the charges become weaker as the charge separation is reduced since the charges become further embedded within the rod. The fluid to string-fluid boundaries also shift towards lower temperatures as the charge separation is reduced for the same reason.

The novel aspects of our contribution are the following. While others have investigated how the rod aspect ratio affects the phase behavior[27,34] we instead focus solely on the internal charge separation. We find that coarse gel-like structures form at high charge separations while denser aggregates form at low charge separations. This suggests that in order to readily form low volume fraction gel structures, the internal charge separation within dipolar colloidal particles should be large as possible.

We find triangularly connected networks at charge separation 3.0, which may be of use for encapsulating smaller particles. An intriguing gel coarsening transition occurs for the two largest charge separations investigated, which suggests using temperature to control the density of a gel of rod-like colloidal particles. Our simulations illustrate how the area fractions, connectivity and coarseness of gel structures can be tuned on the basis of the type of rod-like particles undergoing assembly. The structures formed in our simulations could constitute model systems for low volume fraction gels or materials whose properties (*e.g.* viscosity, conductivity, *etc.*) are controllable by dialing in the core–shell parameters for the individual colloidal particles or the strength of the magnetic or electric field polarization.

By determining which self-assembled structures our dipolar rods can possibly form and at what conditions, we have aided our experimental colleagues in determining the types of phases and structures which will form from various synthesized core–shell rod-like particles. An example of such a core–shell particle is a ferromagnetic nanorod with an inorganic shell overcoat, the thickness of which could determine whether these magnetic dipoles form head-to-tail or side-by-side structures, *i.e.*, the relevant regions on Fig. 2.[42] The magnitude of the dipole could be controlled by the changing the strength of the external field, leading to the polarization of the ferromagnetic core. Though the structures formed at low temperatures in our simulations may not be equilibrium states, they may still represent states which could be experimentally accessible through rapid cooling or rapid gel-formation after momentary magnetic polarization.

Our use of DMD and a rod model with short range interactions was motivated by our desire to highlight regions of the phase diagram for further investigation by experimentalists. This combination of model and simulation technique allowed us to investigate these complex particles quickly and efficiently. The main advantage of DMD is the limited computational resources required (a single processor workstation) in comparison to simulation techniques which use continuous potentials. While the speed of continuous potential simulation techniques has increased through the creation of parallel algorithms, DMD still allows us to simulate more systems in a short time frame given limited computational resources. Though our simulations focused on situations with high salt concentration where short-range interactions were appropriate, it is interesting that the aggregate structures obtained from our simulations appear similar to those obtained in simulations employing long range interactions. Accounting for long range continuous potentials is often the most time consuming part of a simulation; obtaining results which could be qualitatively correct *via* short range potentials is an attractive idea.[48]

The structures formed in our simulations appear consistent with those found by others who have simulated dipolar rods. For instance, McGrother *et al.* found that dipolar rods with an embedded point dipole form S–S structures when the aspect ratio is greater than or equal to 2 : 1 and H–T structures when the aspect ratio is smaller.[26] Varying the aspect ratio of a rod with a point-dipole is equivalent to exploring the x axis in our Fig. 2; the switch between H–T and S–S on this line occurs at an aspect ratio of approximately 1.30 : 1, which is consistent with what McGrother *et al.* had found. Simulations by Aoshima and Satoh of dipolar rods with an extended dipole form H–T and S–S structures as well as higher order structures including triangular and double chain structures.[36] By simulating rods of several aspect ratios with the same difference between rod length and charge separation, they found that the structures formed in their simulations switched from H–T dominated to S–S dominated as the aspect ratio increased. Their systems would fall on a line parallel to the boundary between the H–T favored and the infeasible region in Fig. 2. According to Fig. 2, all three of their charge separations would be in the S–S favorable region. This suggests that if we were to simulate the same particles we would likely obtain different results from Aoshima and Satoh, and our system would be predominately S–S structures and would not switch to an H–T dominated system. Our results also appear to be consistent with simulations of magnetic nanorods composed of fused dipolar spheres performed by Alvarez and Klapp.[27] They do not find nematic order at our aspect ratio regardless of the interaction energy and their percolation transitions occur at decreasing volume fraction as the interaction energy is increased (temperature decreased).

Since the type of behavior observed, phase separation or self-assembly into chains, has been found to depend on the type of model used, at least for dipolar spheres, it is instructive to compare the types of behaviors that we observe for dipolar rods with those observed using other models.[37] Grand canonical Monte Carlo simulations of hard sphere point dipoles,[49] Wang–Landau simulations of Stockmayer fluids with high dipole strength,[50] and Monte Carlo simulations of hard sphere extended dipoles[37] all result in the formation of chains of particles, while simulations of the Stockmayer fluid with low dipole strength appear to exhibit vapor–liquid equilibrium.[51] Both simulations of dipolar spherocylinders and dipolar dumbbells have found ranges of aspect ratios where vapor–liquid coexistence occurs.[26,52,53] Since our model does not include a Stockmayer-like potential and our aspect ratio is significantly above the aspect ratio where spherocylinders display vapor–liquid coexistence, we would expect that our simulations would not display vapor–liquid equilibrium and would instead form chains of particles.

Though small, the differences between the model used in our simulations and a true spherocylinder could potentially lead to anomalous behavior. The percent difference in area between a spherocylinder and the rod used in our simulation is 3.44% due to small gaps between the spheres in our model. If these gaps are too large, they could cause the rods to stack in an offset manner or potentially cause the rods to have a more difficult time sliding past each other at high area fractions. Donaldson and Kantorovich have encountered an analogous situation where cubes constructed from spheres were found to stack closer to each other than true cubes would; these authors surmise that this is the cause of the slight discrepancy observed between their theory and simulation results.[54] We have not,

however, observed our rods stacking in an offset manner in our simulations. Unlike many rod models, ours is not infinitely stiff. This may allow rod particles in our simulations to diffuse past each other more easily than true spherocylinders would. However, we have calculated the persistence length of our rods without charges to be $38.7\sigma \pm 2.6\sigma$, which is significantly higher than our rod length of 4.0σ.

One issue with all of our simulations is whether the structures we measure are equilibrium in nature or simply long lived transient states. The low area fraction non-percolated structure in Fig. 9 in particular suggests that we are not reaching a true equilibrium state since the clusters do not aggregate together even though there is seemingly nothing keeping them apart. For the conditions in this region (charge separation 3.5, low area fraction, low temperature) in particular we ran simulations which were twice as long but we were unable to obtain appreciably different results. From this, we cannot rule out that our simulations may simply be long lived transient states, and our phase diagrams are therefore not describing equilibrium structures. We suggest that our simulations may be limited by both the tight bonding we had to implement in order to maintain a rigid rod shape and the implementation of our Andersen thermostat which tended to slow down the dynamics of the system. Simulations using a rigid rod with a different thermostat may have a higher chance of reaching a state more suggestive of equilibrium.

Appendix

We designed the discontinuous charge–charge potential to mimic the Yukawa potential by matching the discontinuous and continuous total potential between a pair of dipolar rods, the "rod–rod potential", over a variety of configurations. The rod–rod potential is the sum of the four interactions between the positive and negative charges on a pair of rods, not counting interactions between charges on the same rod. We investigated the rod–rod continuous potential as a function of the angle between two adjacent rods, the so called "joint" angle, γ, as described by Alvarez *et al.*[27] This angle is defined as $\gamma = \theta/\pi$, where θ is the angle between the two rods *i.e.* the rods are in a side-by-side alignment when $\gamma = 1$ and are in head–tail alignment when $\gamma = 0$ as shown at the top of Fig. 10. Fig. 10 displays the rod–rod continuous potential *versus* γ as dashed lines for charge separations of 3.0 (blue), 3.5 (red), and 3.7 (black). The corresponding rod–rod discontinuous potentials are shown in solid lines and were calculated using the continuous potential given in eqn (1) of the main text. In order to capture both head–tail and side–side tendencies it was essential that the rod–rod discontinuous potential be a good approximation to the rod–rod continuous potential at charge separations both above and below the dashed line in Fig. 2. The goal, therefore, was to develop a discontinuous rod–rod potential which matched the continuous one at extreme values of γ to give correct energies for head-to-tail and side-by-side arrangements of the dipoles.

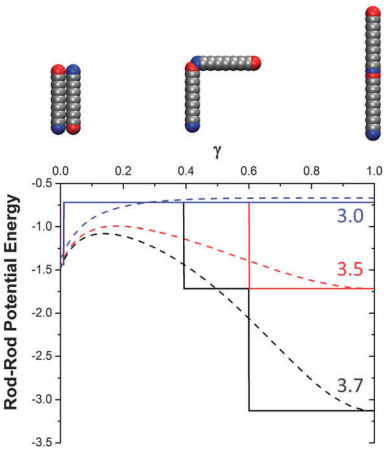

Fig. 10 The rod–rod potential energy *vs.* "joint" angle curves for the Yukawa potential (dashed lines) and our discontinuous potential (solid lines). The three-step discontinuous potential used in our simulations was derived by matching the rod–rod potential energy calculated for the continuous Yukawa potential with that for the discontinuous potential. Black, red and blue lines are for charge separation 3.7, 3.5 and 3.0, respectively.

We chose the locations for the discontinuities in our discontinuous charge–charge potential using the following approach. For a charge separation of 3.7 we wanted a discontinuity in the discontinuous rod–rod potential at $\gamma = 0.6$ because this is approximately the angle at which an inflection point occurs for the continuous rod–rod potential as seen in Fig. 10. This required a discontinuity in the charge–charge potential at a reduced charge–charge distance of 0.595. Similarly, at a charge separation of 3.5 we needed a discontinuity at $\gamma = 0.6$ which required a discontinuity in the charge–charge potential at a reduced charge distance of 0.433. In addition to creating a discontinuity in the rod–rod potential for a charge separation of 3.5 this generated a discontinuity in the rod–rod potential for charge separation 3.7 at a γ of approximately 0.4. Our final discontinuity was chosen to match the rod–rod potential for all three charge separations at $\gamma = 0$. We arbitrarily chose a reduced charge–charge distance of 1.1 for this discontinuity in order to hold the rods "tightly" in a side–side configuration and this generated a discontinuity in the rod–rod potential at small γ values. This defines the three discontinuities used in our model charge–charge potential.

We chose the depths (heights) of the square well (square shoulder) charge–charge potential using the following approach. We forced the depth of the innermost well in our charge–charge potential to take a value of -3.129, the value of the continuous rod–rod potential at $\gamma = 1$ for charge separation 3.7 as shown by the black dashed line in Fig. 10. Similarly, we set the depth of the middle well for the charge–charge potential to be -1.717 so that the discontinuous rod–rod potential would match the continuous potential at $\gamma = 1$ for charge separation 3.5. We set the depth of the outermost well to be -0.719, half the value of the average rod–rod continuous potential at $\gamma = 0$, since there are two charge pairs within this distance, in order to match to the continuous rod–rod potential for the three charge separations at $\gamma = 0$. This completes the definition of the charge–charge discontinuous potential used in our simulations.

Acknowledgements

This work was supported by the Research Triangle MRSEC under grant number DMR-1121107, the US National Science Foundation under grant OISE 1065466 and the German Research Foundation (DFG) through grant IRTG 1524.

Notes and references

1 S. Mitragotri and J. Lahann, *Nat. Mater.*, 2009, **8**, 15–23, DOI: 10.1038/NMAT2344.
2 F. Caruso, R. A. Caruso and H. Mohwald, *Science*, 1998, **282**, 1111–1114, DOI: 10.1126/science.282.5391.1111.
3 D. A. Giljohann, D. S. Seferos, W. L. Daniel, M. D. Massich, P. C. Patel and C. A. Mirkin, *Angew. Chem., Int. Ed.*, 2010, **49**, 3280–3294, DOI: 10.1002/anie.200904359.
4 S. Kredentser, O. Buluy, P. Davidson, I. Dozov, S. Malynych, V. Reshetnyak, K. Slyusarenko and Y. Reznikov, *Soft Matter*, 2013, **9**, 5061–5066, DOI: 10.1039/c3sm27881f.
5 Y. Li, W. Cai and G. Duan, *Chem. Mater.*, 2008, **20**, 615–624, DOI: 10.1021/cm701977g.
6 A. Hynninen, J. H. J. Thijssen, E. C. M. Vermolen, M. Dijkstra and A. Van Blaaderen, *Nat. Mater.*, 2007, **6**, 202–205, DOI: 10.1038/nmat1841.
7 J. Baumgartl, M. Zvyagolskaya and C. Bechinger, *Phys. Rev. Lett.*, 2007, **99**, 205503, DOI: 10.1103/PhysRevLett.99.205503.
8 Y. Chen, X. Ding, S. S. Lin, S. Yang, P. Huang, N. Nama, Y. Zhao, A. A. Nawaz, F. Guo, W. Wang, Y. Gu, T. E. Mallouk and T. J. Huang, *ACS Nano*, 2013, **7**, 3306–3314, DOI: 10.1021/nn4000034.
9 D. J. Milliron, S. M. Hughes, Y. Cui, L. Manna, J. B. Li, L. W. Wang and A. P. Alivisatos, *Nature*, 2004, **430**, 190–195, DOI: 10.1038/nature02695.
10 C. L. Phillips, E. Jankowski, B. J. Krishnatreya, K. V. Edmond, S. Sacanna, D. G. Grier, D. J. Pinei and S. C. Glotzer, *Soft Matter*, 2014, **10**, 7468–7479, DOI: 10.1039/c4sm00796d.
11 B. Bharti and O. D. Velev, *Langmuir*, 2015, **31**, 7897–7908, DOI: 10.1021/la504793y.
12 P. Bolhuis and D. Frenkel, *J. Chem. Phys.*, 1997, **106**, 666–687, DOI: 10.1063/1.473404.
13 M. J. Solomon and P. T. Spicer, *Soft Matter*, 2010, **6**, 1391–1400, DOI: 10.1039/b918281k.
14 A. Walther and A. H. E. Mueller, *Soft Matter*, 2008, **4**, 663–668, DOI: 10.1039/b718131k.
15 A. A. Shah, B. Schultz, W. Zhang, S. C. Glotzer and M. J. Solomon, *Nat. Mater.*, 2015, **14**, 117–124, DOI: 10.1038/NMAT4111.
16 A. Snezhko and I. S. Aranson, *Nat. Mater.*, 2011, **10**, 698–703, DOI: 10.1038/NMAT3083.
17 J. J. Crassous, A. M. Mihut, E. Wernersson, P. Pfleiderer, J. Vermant, P. Linse and P. Schurtenberger, *Nat. Commun.*, 2014, **5**, 5516, DOI: 10.1038/ncomms6516.
18 K. J. Lee, J. Yoon, S. Rahmani, S. Hwang, S. Bhaskar, S. Mitragotri and J. Lahann, *Proc. Natl. Acad. Sci. U. S. A.*, 2012, **109**, 16057–16062, DOI: 10.1073/pnas.1213669109.
19 O. Cayre, V. Paunov and O. Velev, *J. Mater. Chem.*, 2003, **13**, 2445–2450, DOI: 10.1039/b308817k.
20 I. D. Hosein, M. Ghebrebrhan, J. D. Joannopoulos and C. M. Liddell, *Langmuir*, 2010, **26**, 2151–2159, DOI: 10.1021/la902609s.
21 H. Zhang, J. K. Nunes, S. E. A. Gratton, K. P. Herlihy, P. D. Pohlhaus and J. M. DeSimone, *New J. Phys.*, 2009, **11**, 075018, DOI: 10.1088/1367-2630/11/7/075018.
22 S. Maity, W. Wu, C. Xu, J. B. Tracy, K. Gundogdu, J. R. Bochinski and L. I. Clarke, *Nanoscale*, 2014, **6**, 15236–15247, DOI: 10.1039/c4nr05179c.
23 J. Yan, K. Chaudhary, S. C. Bae, J. A. Lewis and S. Granick, *Nat. Commun.*, 2013, **4**, 1516, DOI: 10.1038/ncomms2520.
24 D. Fava, Z. Nie, M. A. Winnik and E. Kumacheva, *Adv. Mater.*, 2008, **20**, 4318–4322, DOI: 10.1002/adma.200702786.
25 D. Fava, M. A. Winnik and E. Kumacheva, *Chem. Commun.*, 2009, 2571–2573, DOI: 10.1039/b901412h.
26 S. McGrother and G. Jackson, *Phys. Rev. Lett.*, 1996, **76**, 4183–4186, DOI: 10.1103/PhysRevLett.76.4183.
27 C. E. Alvarez and S. H. L. Klapp, *Soft Matter*, 2012, **8**, 7480–7489, DOI: 10.1039/c2sm25636c.
28 C. E. Alvarez and S. H. L. Klapp, *Soft Matter*, 2013, **9**, 8761–8770, DOI: 10.1039/c3sm51549d.
29 M. A. Miller, R. Blaak, C. N. Lumb and J. Hansen, *J. Chem. Phys.*, 2009, **130**, 114507, DOI: 10.1063/1.3089620.
30 H. Schmidle, C. K. Hall, O. D. Velev and S. H. L. Klapp, *Soft Matter*, 2012, **8**, 1521–1531, DOI: 10.1039/c1sm06576a.
31 H. Schmidle, S. Jaeger, C. K. Hall, O. D. Velev and S. H. L. Klapp, *Soft Matter*, 2013, **9**, 2518–2524, DOI: 10.1039/c2sm27210e.
32 A. Goyal, C. K. Hall and O. D. Velev, *Phys. Rev. E: Stat., Nonlinear, Soft Matter Phys.*, 2008, **77**, 031401, DOI: 10.1103/PhysRevE.77.031401.
33 A. Goyal, C. K. Hall and O. D. Velev, *Soft Matter*, 2010, **6**, 480–484, DOI: 10.1039/b907873h.
34 M. Aoshima and A. Satoh, *J. Colloid Interface Sci.*, 2004, **280**, 83–90, DOI: 10.1016/j.jcis.2004.07.025.
35 V. Ballenegger and J. P. Hansen, *Mol. Phys.*, 2004, **102**, 599–609, DOI: 10.1080/00268970410001675554.
36 M. Aoshima and A. Satoh, *J. Colloid Interface Sci.*, 2006, **293**, 77–87, DOI: 10.1016/j.jcis.2005.06.035.
37 M. Valisko, T. Varga, A. Baczoni and D. Boda, *Mol. Phys.*, 2010, **108**, 87–96, DOI: 10.1080/00268970903514553.
38 S. Gangwal, O. J. Cayre, M. Z. Bazant and O. D. Velev, *Phys. Rev. Lett.*, 2008, **100**, 058302, DOI: 10.1103/PhysRevLett.100.058302.
39 W. Wu and J. B. Tracy, *Chem. Mater.*, 2015, **27**, 2888–2894, DOI: 10.1021/cm504764v.
40 A. Bellemans, J. Orban and D. Vanbelle, *Mol. Phys.*, 1980, **39**, 781–782, DOI: 10.1080/00268978000100671.
41 J. Bergenholtz and M. Fuchs, *J. Phys.: Condens. Matter*, 1999, **11**, 10171–10182, DOI: 10.1088/0953-8984/11/50/310.
42 K. A. Kozek, K. M. Kozek, W. Wu, S. R. Mishra and J. B. Tracy, *Chem. Mater.*, 2013, **25**, 4537–4544, DOI: 10.1021/cm402277y.
43 J. N. Israelachvili, *Intermolecular and surface forces*, Academic Press, Burlington, MA, 2011.

44 H. Andersen, *J. Chem. Phys.*, 1980, **72**, 2384–2393, DOI: 10.1063/1.439486.
45 H. Neitsch and S. H. L. Klapp, *J. Chem. Phys.*, 2013, **138**, 064904, DOI: 10.1063/1.4790406.
46 M. Li, H. Schnablegger and S. Mann, *Nature*, 1999, **402**, 393–395.
47 M. A. Bates and D. Frenkel, *J. Chem. Phys.*, 2000, **112**, 10034–10041, DOI: 10.1063/1.481637.
48 C. J. Fennell and J. D. Gezelter, *J. Chem. Phys.*, 2006, **124**, 234104, DOI: 10.1063/1.2206581.
49 P. Camp, J. Shelley and G. Patey, *Phys. Rev. Lett.*, 2000, **84**, 115–118, DOI: 10.1103/PhysRevLett.84.115.
50 G. Ganzenmueller and P. J. Camp, *J. Chem. Phys.*, 2007, **127**, 154504, DOI: 10.1063/1.2794042.
51 H. Schmidle and S. H. L. Klapp, *J. Chem. Phys.*, 2011, **134**, 114903, DOI: 10.1063/1.3564916.
52 J. C. Shelley, G. N. Patey, D. Levesque and J. J. Weis, *Phys. Rev. E: Stat. Phys., Plasmas, Fluids, Relat. Interdiscip. Top.*, 1999, **59**, 3065–3070, DOI: 10.1103/PhysRevE.59.3065.
53 G. Ganzenmuller and P. J. Camp, *J. Chem. Phys.*, 2007, **126**, 191104, DOI: 10.1063/1.2738059.
54 J. G. Donaldson and S. S. Kantorovich, *Nanoscale*, 2015, **7**, 3217–3228, DOI: 10.1039/c4nr07101h.